Humidity effect on BaTiO$_3$ *c*-domain surface potential inversion induced by electric field

D. Y. He,[1] L. J. Qiao,[1] and Alex A. Volinsky[1,2]

[1]*Corrosion and Protection Center, Key Laboratory for Environmental Fracture (MOE),*
University of Science and Technology Beijing, Beijing 100083, People's Republic of China
[2]*Department of Mechanical Engineering, University of South Florida, Tampa Florida 33620, USA*

The potential distribution of ferroelectric domains on a (001) BaTiO$_3$ single crystal surface was investigated via scanning Kelvin probe microscopy at room temperature, with and without an electric field applied parallel to the (001) surface. A reversal of the *c* domain charge was observed after reaching a critical electric field intensity of 6 V/mm, which was much lower than the 200 V/mm coercive field. An immediate recovery was observed upon switching off the electric field. The humidity has a significant effect on the intensity of the inversion electric field. Surface adsorbates significantly affected the ferroelectric surface potential behavior. Due to a low 4 kJ/mol desorption energy, the electric field successfully removed surface adsorbates, allowing for the surface potential to reflect the actual domain polarization state. © *2011 American Institute of Physics.* [doi:10.1063/1.3636396]

I. INTRODUCTION

Ferroelectric perovskite oxide domain patterns are related to spontaneous polarization[1] and surface charge. As such, the domain charge is reflected in surface potential images.[2] Scanning probe microscopy (SPM) is a powerful method for observing domain structures, and their dynamic behavior, on ferroelectric surfaces.[3–9] As a simple and convenient method, SPM is widely used to characterize topography features, chemical reactivity, and adsorbed species.[10–19] Compared to other SPM modes, the Kelvin probe SPM is more sensitive to electrostatic forces, which can be used to detect the ferroelectric surface potential distribution.[20,21]

The SPM of domain and surface potential characterizations in ferroelectrics has been reported.[10–13] These studies dealt with adsorbates on perovskite surfaces, with some even reporting surface potential inversion. Kalinin *et al.* showed a temperature-induced potential inversion on a (001) BaTiO$_3$ single crystal surface.[18] Liu *et al.* observed surface potential inversion after heating a LiNbO$_3$ single crystal.[19] These results demonstrate that adsorbates are indeed present on polarized ferroelectric surfaces and therefore affect surface potential measurements. Thus, the influence of surface adsorbates should be taken into account. Indeed, in the case of ferroelectrics, surface properties are affected by the presence of adsorbed layers, making it difficult to characterize the actual domain charge states. This calls for a better understanding of domain polarization and surface adsorption behavior.

Here, an overall investigation of the surface potential reversal of ferroelectric domains in a BaTiO$_3$ single crystal, upon applying a parallel electric field, is reported. Such phenomenon was observed from ferroelectric *c* domains, with spontaneous polarization pointing either upward or downward, with respect to the observed (001) surface. The domain size, the direction of the applied electric field, the surrounding domain, and even the relative humidity effects were all considered in the experiments. Being driven by an applied electric field, the charge associated with physisorption was completely removed, which then allowed for the characterization of the domain polarization via surface potential imaging.

II. EXPERIMENTAL DETAILS

A commercial, zero degree cut, undoped BaTiO$_3$ single crystal with ⟨001⟩ orientation and $4 \times 3 \times 1$ mm^3 dimensions was used in this study. At room temperature, BaTiO$_3$ exhibits tetragonal symmetry as the Ti ions shift with respect to the oxygen octahedral, resulting in a spontaneous polarization either parallel or perpendicular to the observed (001) surface. Domains with the polarization vector aligned perpendicular to the crystal surface are defined as *c* domains with respect to the (001) surface. Similarly, domains with the polarization vector aligned parallel to the crystal (001) surface are defined as *a* domains. Here, the crystal was poled along the [100] direction to get the *a* domains on the observed (001) plane and the surface was polished to less than 1 nm roughness. The (001) surface was carefully polished by diamond lapping pastes with sizes ranging from w2.5 to w0.5. To reduce the surface roughness and achieve good AFM image contrast, the sample was further polished using a 50 nm colloidal silica suspension, resulting in 10 Å surface roughness. The sample was cleaned supersonically in deionized water. After that, to obtain a multi-domain structure on the BaTiO$_3$ (001) surface, the sample was annealed in air, at 110 °C for 2 h, prior to the ferroelectric and paraelectric phase transitions at its 120 °C Curie temperature. The crystal was then heated to 135 °C for 30 min in air to achieve a steady homogeneous state, and was cooled to room temperature in air, at a rate of 100 °C/min. In this way, the polarized domain structure containing *a*, *c*$^+$, and, *c*$^-$ domains was achieved (Fig. 1). The domains with spontaneous polarization vectors along the [100], [001], and [00$\bar{1}$] directions, with respect to the (001) surface, are regarded as *a*, *c*$^+$, and *c*$^-$ domains, respectively. Figures 1(a) and 1(b) show
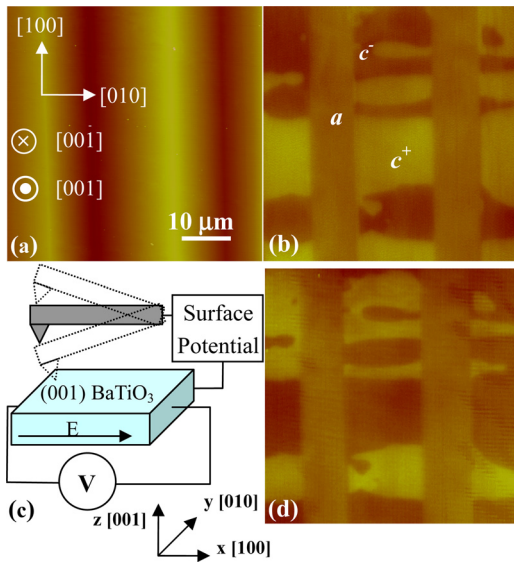
FIG. 1. (Color online) (a) AFM topography image of the $BaTiO_3$ (001) surface. The Z scale is 200 nm. (b) Surface potential image without voltage applied or at 4 V/mm electric field intensity. (c) Schematic of the surface potential measurement with applied electric field. (d) Surface potential image after applying 6 V/mm electric field intensity showing potential inversion.

topography and surface potential maps of the $BaTiO_3$ (001) surface, respectively. The corrugated topography is attributed to adjacent a and c domains, induced by the 0.6° orientation difference at room temperature. The 90° a-c domain walls appear as straight lines on the (001) surface, parallel to the [100] direction.

Since the c domain has a polarization vector pointing either upward (c^+) or downward (c^-), with respect to the (001) plane, the polarization charge is therefore generated on the surface. The dark regions within the c domain have a negative potential and correspond to c^- domains, while the surrounding bright regions have a positive potential and thus correspond to c^+ domains. The 180° c^+-c^- domains are separated by irregularly curved domain walls and have no observable corrugation between each other, as can be seen in the topography images. The a domain polarization vector is in the (001) plane and thus has no surface charge. As such, its contrast is in-between those of the c^+ and c^- domains. Consequently, the bright, dark and intermediate regions correspond to the c^-, c^+, and a domains, respectively, with a 100 mV difference existing between the c^+ and c^- domains.

The surface potential measurements were carried out with a Digital Instruments Dimension V SPM system (USA) utilizing a W_2C coated tip (NSG01/W_2C, NT-MDT, Russia). The experiments were performed at 135 kHz, just below the 150 kHz cantilever resonance frequency. The lift scan height in the interleave control was 100 nm. An oscillating voltage $V_{ac}\cos(\omega t)$ was applied directly to the cantilever tip and was used for surface potential measurements. In these studies, the driving voltage V_{ac} was 1500 mV, with a scan rate of 1 Hz and a 10 min image capture time.

The external electric field (E) was applied paralleled to (001) surface, i.e. along the [100] direction, as shown sche-

matically in Fig. 1(c). By coating silver paste electrodes on both sides of the sample, a voltage source was connected using copper wires. This allowed simultaneous electric field application and surface potential measurement so that local domain polarization evolution could be studied.

III. RESULTS AND DISCUSSION

The AFM topography of the $BaTiO_3$ single crystal is shown in Fig. 1(a). During testing, topography images did not change. The local surface potential images, while applying a 4 V/mm and a 6 V/mm electric field intensity, are shown in Fig. 1(b) and Fig. 1(d), respectively. Figure 1(b), with a 4 V/mm electric field intensity, looks exactly the same as the original surface potential distribution, without the electric field applied. One-hour of continued scanning was conducted for each electric field intensity. The applied voltage was then continuously increased to 18.2 V, corresponding to the 6 V/mm electric field intensity. At that time, the measured c domain surface potential reversed its sign, as seen in Fig. 1(d), demonstrating a complete c domain sign inversion. The variation of the surface potential can be seen by comparing Figs. 1(b) and 1(d). Here, the bright positive charge areas become dark negative. Above the 6 V/mm critical field intensity, which is two orders of magnitude lower than the 200 V/mm coercive field,[22,23] no further change in the surface potential was observed. Experiments with opposite electric fields were also carried out. Switching the applied electric field polarity produces the same result, meaning that the surface potential inversion has no relation with the applied electric field direction.

Furthermore, the surface potential recovered when the electric field was reduced below the critical reversal value. In Fig. 2, the surface potential recovery was observed when the applied electric field was removed, where both the sign and magnitude of the c^+ and c^- domains were restored to their original values. This process is fully reversible.
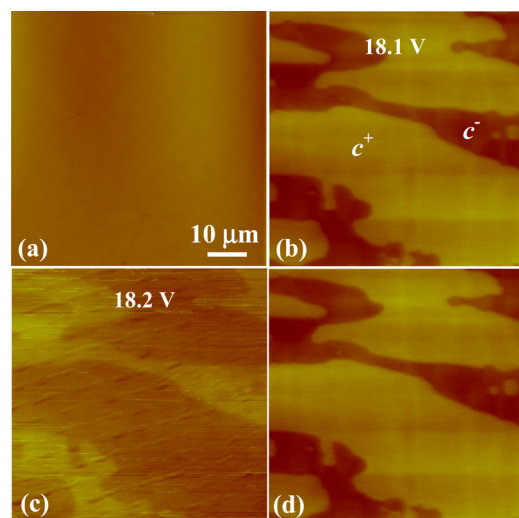
FIG. 2. (Color online) (a) Topography image of the c domain with the 200 nm Z scale. Surface potential map of the c domain at (b) 18.1 V and (c) 18.2 V showing surface potential inversion. (d) Complete recovery upon switching the electric field off.

In order to analyze the local surface potential distribution, only the *c* domain area was measured, thereby avoiding the impact of the *a* domains. Figures 2(a) and 2(b) show the *c* domain surface topography and the original surface potential images, without an electric field applied. Figure 2(b) shows the surface potential distribution of the *c* domain, although its surface topography is uniform in Fig. 2(a). The corresponding surface potential regions did not change when the applied electric field intensity was lower than 6 V/mm. As soon as the applied electric field intensity reached the threshold value of 6 V/mm, the surface potential immediately reversed, as can be seen in Fig. 2(c). The ripples in Fig. 2(c) are noise caused by the electric field and are not related to the intrinsic domain structure. Apparently, the surface potential inversion has no relationship with the domain size.

In order to investigate the sensitivity of the surface potential to the applied electric field, the applied voltage was changed during image capture. Figure 3(a) shows the surface potential map of the 180° *c* domain zone before the applied electric field reached the critical reversal intensity. Here, a smaller c^- domain is embedded in the surrounding c^+ domain. Figure 3(b) shows that, after the applied electric field reached the critical value, the surface potential inverted. From repeated experiments, it became apparent that the critical voltage is between 18.1 V and 18.2 V. As such, the applied voltage was repeatedly changed between 18.1 V and 18.2 V, back and forth, as can be seen, along with the corresponding surface potential profile, in Fig. 3(c). The left sec-

tion was imaged at an applied voltage of 18.1 V. After scanning for a short time, the voltage was increased to 18.2 V, whose consequent surface potential profile can be seen in the second part of the image. The surface potential distribution changed with the applied voltage. On the right-hand side of the image in Fig. 3(c), the positive and negative charge areas can be seen to coexist, as outlined by their respective surface potential profiles.

The surface potential inversion, caused by small changes in electric field, was further investigated by varying the relative humidity (RH). The critical reversal electric field intensity initially increased with humidity, showing no change past 45% RH [Fig. 3(d)]. This provides strong evidence that the phenomenon of surface potential inversion is related to surface adsorption.

The $BaTiO_3$ coercive field (E_c), at which domain switching begins, is 200 V/mm.[22,23] However, in our experiments, the surface potential switching electric field intensity is incredibly low, at about 1/40 of E_c. Regardless, with a lower electric field the switching time should be longer. However, such was not the case here, as the apparent switching time was less than a second. The observed inversion was therefore not due to domain switching, but rather to surface screening charge migration.

Charges adsorb on the surface by means of attractive forces originating from oriented dipoles. Adsorbed charges on the oxide surfaces are thus removable. The attractive force has a strong effect on the spread of the ferroelectric surface charge. A low activation energy of 4 kJ/mol (Ref. 18) suggests that immediate desorption can easily happen due to the applied electric field. What was observed is simply a charge diffusion process. When the electric field is switched off, the surface compensation reverts back to the charge screening state. Consequently, the surface potential recovers to its original value, which is to say that the electric field-dependent surface potential mainly relies upon the adsorption and desorption of the surface screening charges. We think that the surface potential inversion is due to the surface charge migration along the direction of the electric field gradient. This is likely the reason for $BaTiO_3$ single crystal surface potential inversion.[24]

It also appears that the critical reversal electric field changed with humidity. As seen in Figs. 3(e) and 3(f), surface potential contrast decreases, meaning that there is more adsorbed water neutralizing surface charges. These results are consistent with the previous work.[25] It was found that at the medium humidity levels the inversion electric field is more affected by the humidity, while at higher humidity the electric field is not as sensitive to the relative humidity variations. The characterization of the humidity impact on the surface potential performance was based on two aspects. At ambient humidity, potential image based upon contrast decreased due to water molecules adsorbed on the surface, and neutralized the *c* domain surface charge. With water adsorbed on the surface, the electric field needed for the potential inversion increased 167% and 238%, respectively, at the two measured humidity levels is compared with the initial values. It is remarkable that neither is the electric field direction nor the sample tested area affected the potential
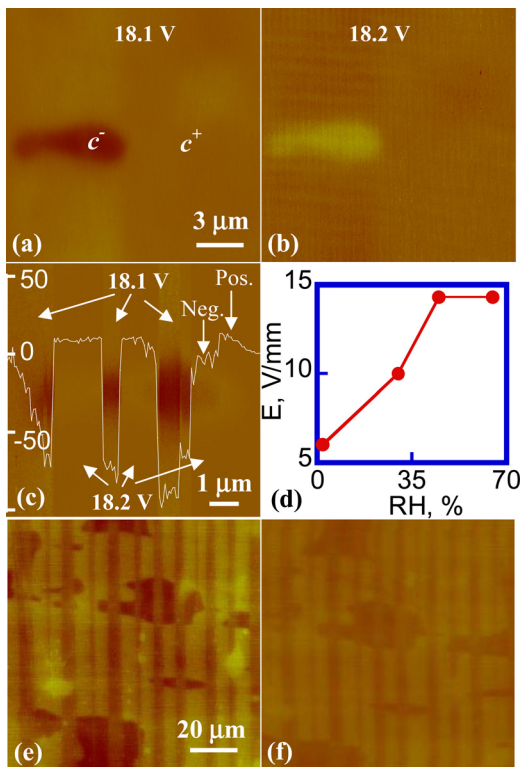
FIG. 3. (Color online) Surface potential mapping on the 180° *c* domain zone with different applied voltage: (a) 18.1 V, (b) 18.2 V, (c) alternating between 18.1 V and 18.2 V with the corresponding potential profile. (d) Reversal electric field intensity dependence on relative humidity. (e) Surface potential images of *a-c* domain patterns on the (001) $BaTiO_3$ single crystal at 2% RH, and (f) 65% RH. Same 0.6 V Z scale for (e) and (f).

inversion behavior. Only relative humidity had an effect on the potential inversion, which can be explained by the higher desorption energy of the surface-trapped water. Chornik *et al.* obtained a high desorption energy of 126 kJ/mol from a thermal desorption experiment on amorphous $BaTiO_3$ thin film surfaces, which can be ascribed to the water dissociation.[26] As deduced before, with the help of the electric field, the mobile screening charges were desorbed from the surface in dry air. However, in the humid ambient, the adsorbed water resulted in additional strong interactions between the water molecules and the surface charges, along with the weak adsorption between the water molecules and the domain polarization underneath. Thus, a larger electric field was needed to remove the top adsorbates, and the critical reversal electric field changed with humidity. At high humidity, interactions between the multilayers of water molecules on the top surface became weaker and weaker, thus the electric field needed for the potential inversion no longer changed. The desorption energy at high RH could be estimated at 2.08 eV (200.7 kJ/mol), whereas at relatively dry conditions the desorption energy is 0.36 eV (34.7 kJ/mol), as deduced from the work function acquired from the surface potential. The observed humidity effect on the surface potential inversion provides strong evidence that the surface potential inversion is related to the surface species adsorption. Thus, it can be concluded that the electrostatic interactions between the ferroelectric domains and the surface-adsorbed species, such as molecule dipoles, trapped electrons, or space charges, are responsible for the surface charge evolution. A larger electric field was therefore needed to remove the adsorbates. It can thus be stated that the screening by adsorbates plays a dominant role in the performance of ferroelectrics.

IV. CONCLUSIONS

In summary, the surface potential evolution of a (001) $BaTiO_3$ single crystal surface, with an electric field applied along the [010] direction, was studied. The surface potential sign of the *c* domains reversed as soon as the applied electric field intensity reached 6 V/mm and then switched back to their original state when the electric field was reduced to below 6 V/mm. The surface potential inversion has no correlation with the direction of the applied electric field or the domain size. Relative humidity, however, has a strong effect on the domain switching behavior. This electric field-dependent

surface potential mainly relies upon the adsorption and desorption of surface screening charges, as they are driven by low activation energy. The surface potential therefore exhibited inversion because of the charge dispersion upon the surface.

[1]D. Vanderbilt, Phys. Rev. B **41**, 7892 (1990).
[2]S. V. Kalinin and D. A. Bonnell, Phys. Rev. B **63**, 125411 (2001).
[3]Y. G. Wang, J. Dec, and W. Kleemann, J. Appl. Phys. **84**, 6795 (1998).
[4]J. Munoz-Saldana, G. A. Schneider, and L. M. Eng, Surf. Sci. Lett. **480**, L402 (2001).
[5]B. Reichenberg, S. Tiedke, K. Szot, F. Peter, R. Waser, S. Tappe, and T. Schneller, J. Eur. Ceram. Soc. **25**, 2353 (2005).
[6]B. J. Rodriguez, R. J. Nemanich, A. Kingon, and A. Gruverman, Appl. Phys. Lett. **86**, 012906 (2005).
[7]Y. B. Park, M. J. Dicken, Z. H. Xu, and X. D. Li, J. Appl. Phys. **102**, 083507 (2007).
[8]O. S. Ovchinnikov, S. Jesse, and S. V. Kalinin, Nanotechnology **20**, 255701 (2009).
[9]S. V. Kalinin, A. N. Morozovska, L. Q. Chen, and B. J. Rodriguez, Rep. Prog. Phys. **73**, 056502 (2010).
[10]S. V. Kalinin and D. A. Bonnell, Appl. Phys. Lett. **78**, 1116 (2001).
[11]S. Shin, J. Baek, J. W. Hong, and Z. G. Khim, J. Appl. Phys. **96**, 4372 (2004).
[12]R. Shao, M. P. Nikiforov, and D. A. Bonnell, Appl. Phys. Lett. **89**, 112904 (2006).
[13]Q. Dai, J. Hu, and M. Salmeron, J. Phys. Chem. B **101**, 1994 (1997).
[14]M. Luna, J. Colchero, and A. M. Baro, J. Phys. Chem. B **103**, 9576 (1999).
[15]M. Luna, J. Colchero, A. Gil, J. Go'mez-Herrero, and A. M. Baro, Appl. Surf. Sci. **175**, 393 (2000).
[16]A. Verdaguer, M. Cardellach, and J. Fraxedas, J. Chem. Phys. **129**, 174705 (2008).
[17]D. B. Li, M. H. Zhao, J. Garra, A. M. Kolpak, A. M. Rappe, D. A. Bonnell, and J. M. Vohs, Nature Mater. **7**, 473 (2008).
[18]S. V. Kalinin, C. Y. Johnson, and D. A. Bonnell, J. Appl. Phys. **91**, 3816 (2002).
[19]X. Y. Liu, K. Kenji, and T. Kazuya, Appl. Phys. Lett. **89**, 132905 (2006).
[20]Q. Zhang, C. H. Kim, Y. H. Jang, H. J. Hwang, and J. H. Cho, Appl. Phys. Lett. **96**, 152901 (2010).
[21]Y. Kim, M. Park, S. Buhlmann, S. Hong, Y. K. Kim, H. Ko, J. Kim, and K. No, J. Appl. Phys. **107**, 054103 (2010).
[22]W. J. Merz, Phys. Rev. **95**, 650 (1954).
[23]A. Ryuji, J. Phys. Soc. Jpn. **15**, 795 (1960).
[24]D. Y. He, L. J. Qiao, A. A. Volinsky, Y. Bai, and L. Q. Guo, Phys. Rev. B **84**, 024101 (2011).
[25]D. Y. He, L. J. Qiao, A. A. Volinsky, Y. Bai, M. Wu, and W. Y. Chu, Appl. Phys. Lett. **98**, 062905 (2011).
[26]B. Chornik, V. A. Fuenzalida, C. R. Grahmann, and R. Labbé, Vacuum **48**, 161 (1997).